Science Advances
AAAS

Supplementary Materials for

The 2023 coastal El Niño: Atmospheric and air-sea coupling mechanisms

Qihua Peng, Shang-Ping Xie*, Gino A. Passalacqua, Ayumu Miyamoto, and Clara Deser

Correspondence to: sxie@ucsd.edu

This PDF file includes:

Table S1
figs. S1 to S13

Table S1. Description of the MITgcm experiments

Experiments	Forcing	Description
CTRL	6-hourly realistic forcing	All processes included
$\boldsymbol{\tau}'_{\mathbf{Coast}}$	Time-varying (climatological) wind stress in (outside) the coastal region (75˚ W- 90˚ W, 20˚ S-5˚ N). All the other forcings are fixed to their daily climatological values.	Impacts of coastal wind anomalies
$\boldsymbol{\tau}'_{\mathbf{EEP}}$	Same as $\boldsymbol{\tau}'_{\mathbf{Coast}}$, but using realistic wind stress in the eastern equatorial Pacific (EEP, 90 ˚ W- 130˚ W, 5˚ S-5˚ N).	EEP anomalous wind effects
$\boldsymbol{\tau}'_{\mathbf{CWP}}$	Same as $\boldsymbol{\tau}'_{\mathbf{Coast}}$, but using realistic wind stress in the western equatorial Pacific (CWP, 120 ˚ E- 130˚ W, 5˚ S-5˚ N).	CWP wind impacts

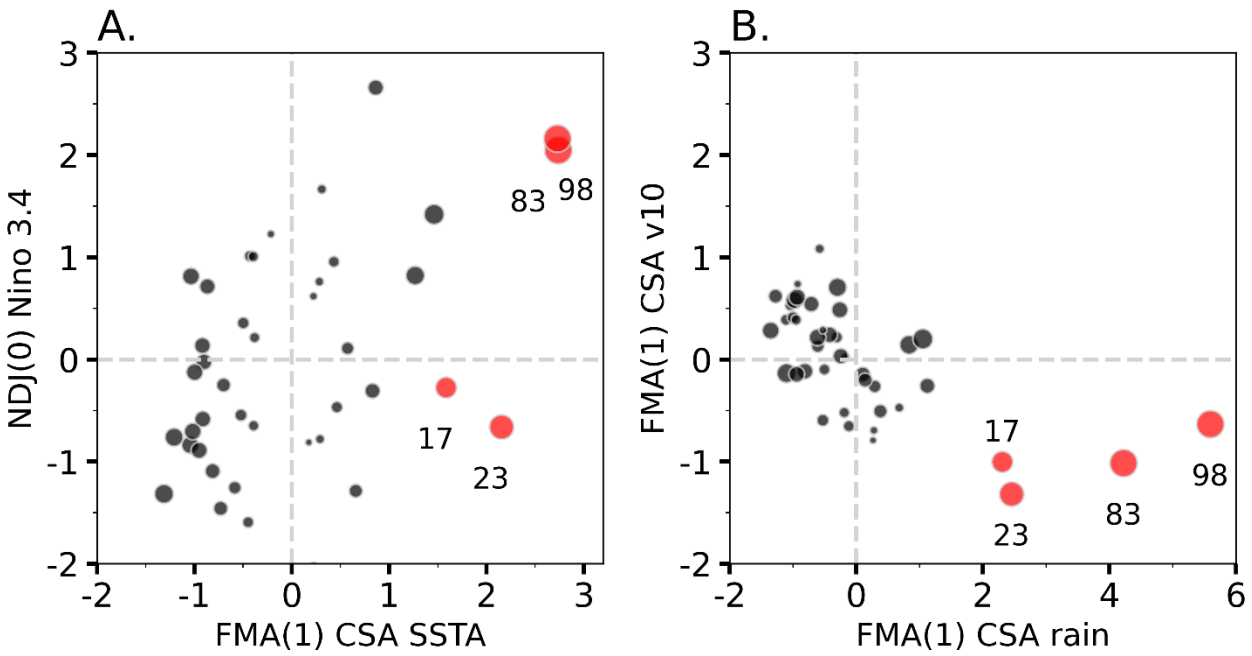

fig. S1. Relationship of basin-scale El Niño with coastal El Niño during 1982-2023. Scatter plot for (A) FMA coastal region of South America (CSA, 85° W – 80° W, 10° S – 0°) SST anomalies (℃) and November-January (NDJ) mean Niño 3.4 anomalies; (B) CSA FMA rainfall anomalies (mm/day) and v10 anomalies (m/s). The size of each point represents the amplitude of SST anomalies in the CSA region.

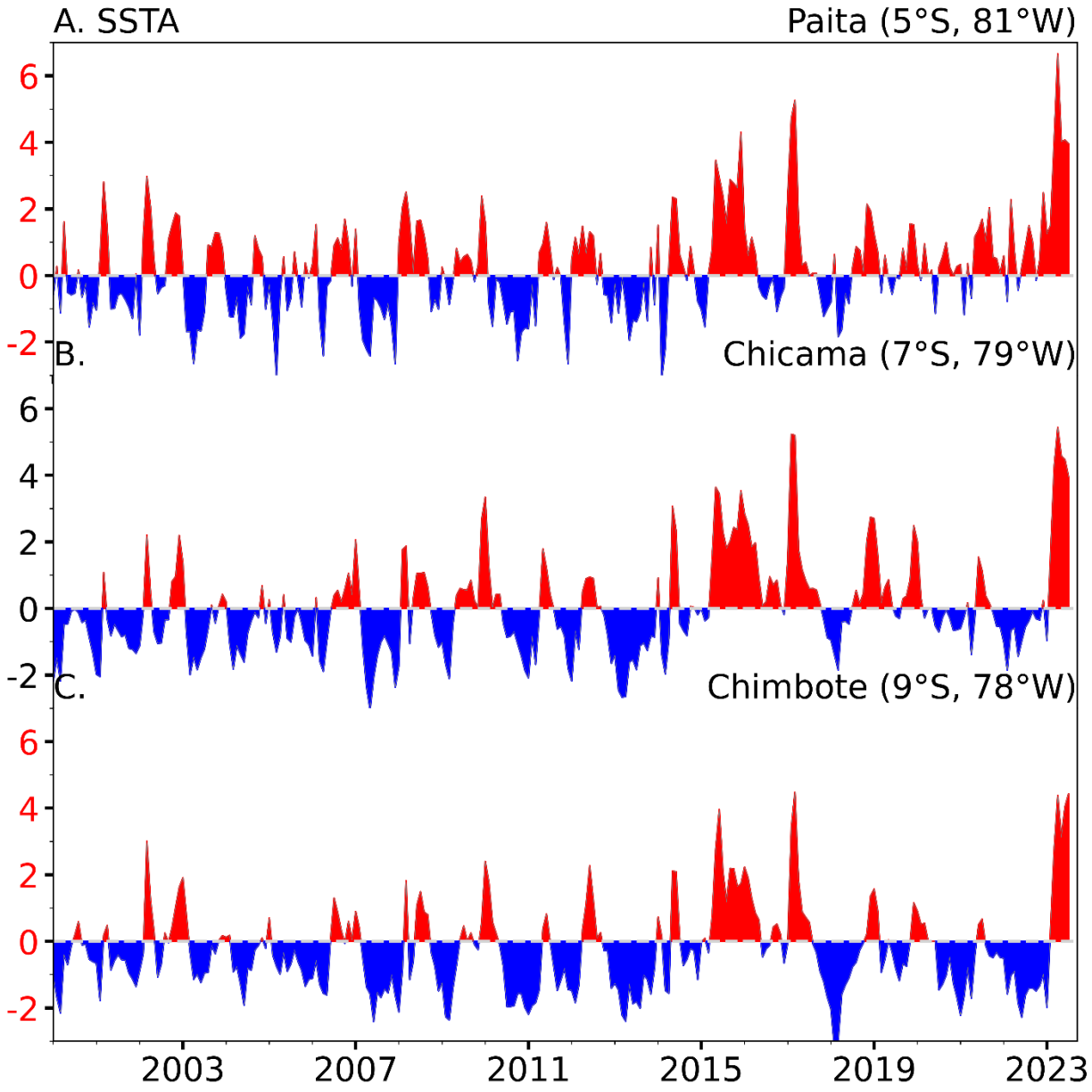

fig. S2. In-situ observed SST anomalies off Peru. Monthly SST anomalies (℃) observed at (A) Paita, (B) Chicama, and (C) Chimbote stations.

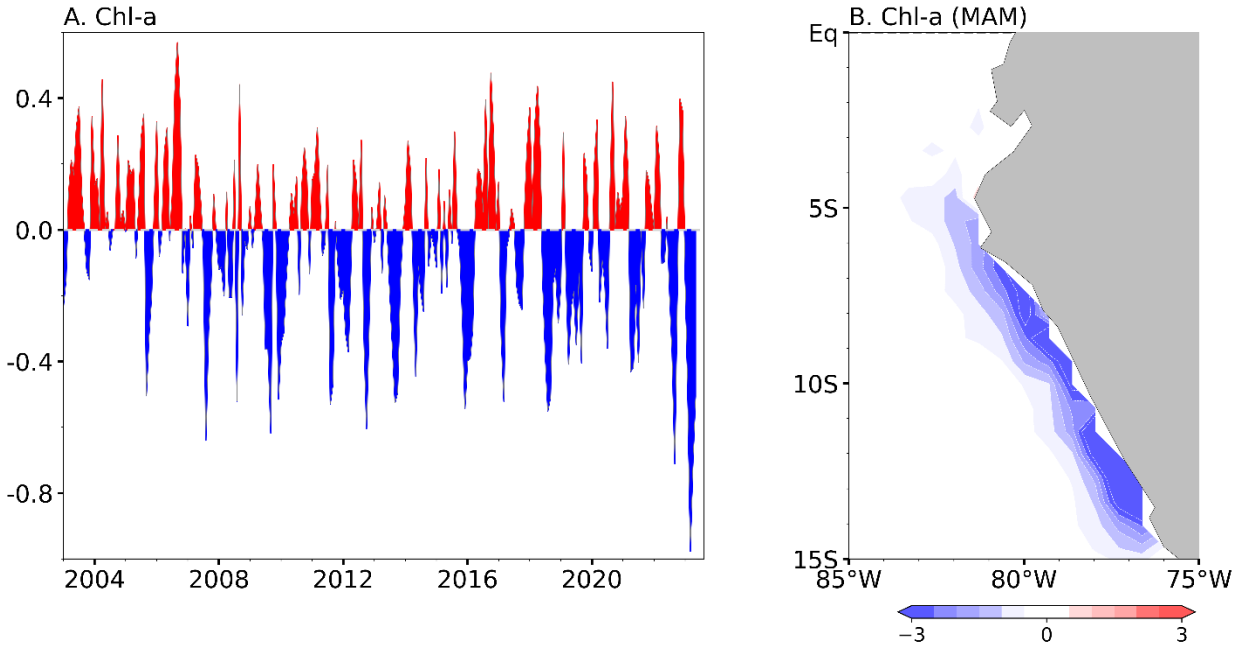

fig. S3. Chl-a anomalies during the 2023 event. (A) Time series of observed Chl-a anomalies (mg/m^3) over the southeastern Pacific coastal region (75 ˚W- 85˚ W, 5˚ S-15˚ S). (B) The spatial pattern of Chl-a anomalies (mg/m^3) averaged in March-May 2023.

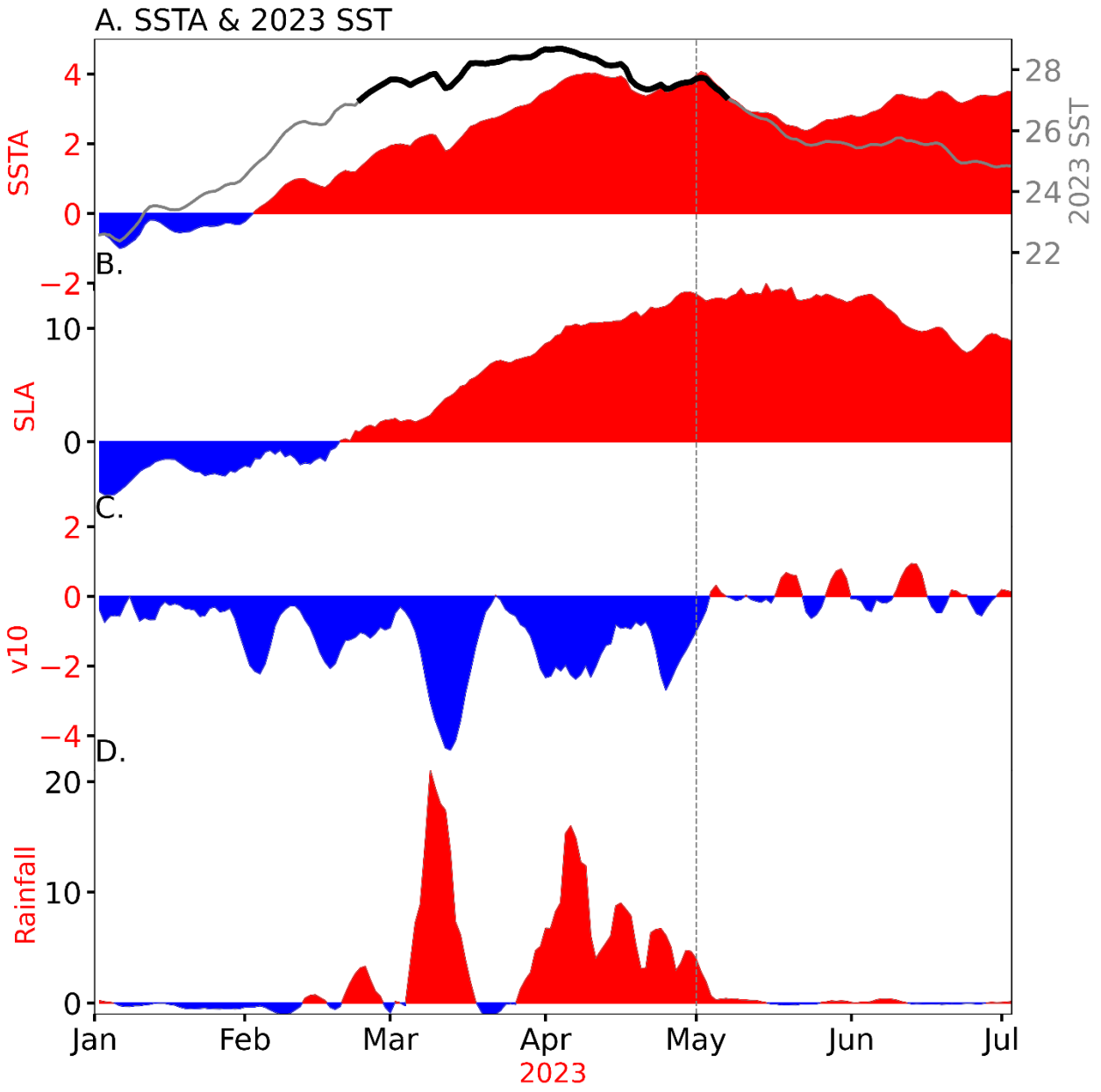

fig. S4. Oceanic and atmospheric anomalies as a function of time for the 2023 coastal El Niño. Time series of daily CSA averaged (A) SST anomalies and SST (grey line, SST>27℃ is highlighted in black), (B) SLA (cm), (C) v10 anomalies (m/s), and (D) rainfall anomalies (mm/day) from January to July 2023.

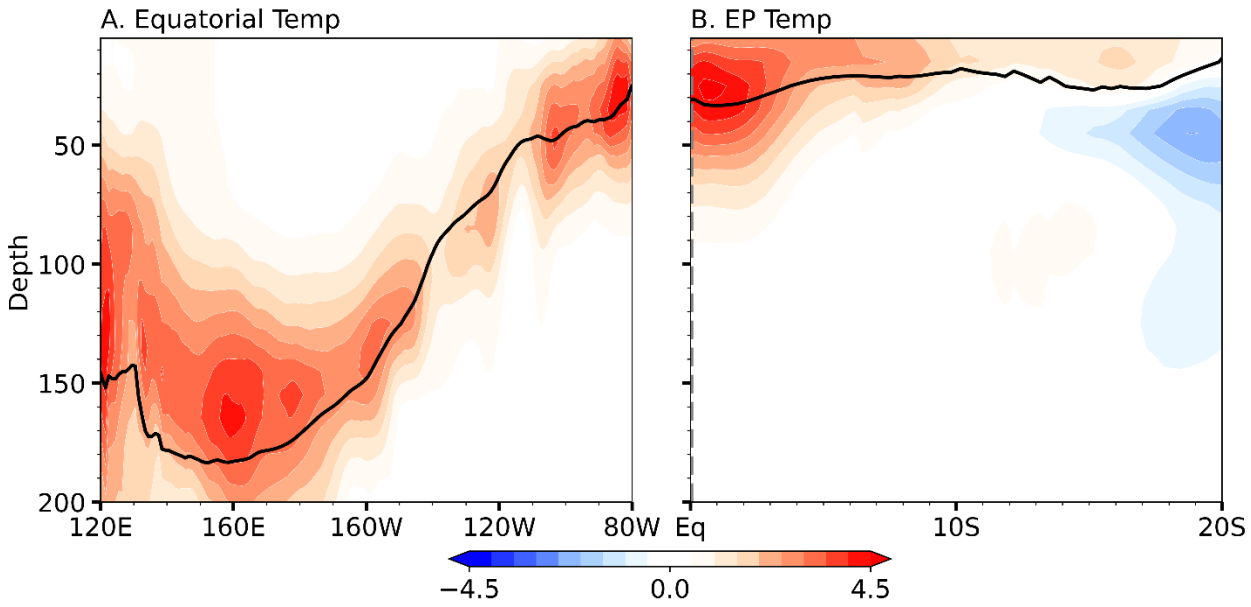

fig. S5. WWV and subsurface perturbations for the 2023 event. March-May (MAM) Observed (A) equatorial and (B) eastern Pacific (zonally averaged in 80°W-85°W) subsurface temperature anomalies (℃). Black line represents the 23 ℃ isotherm.

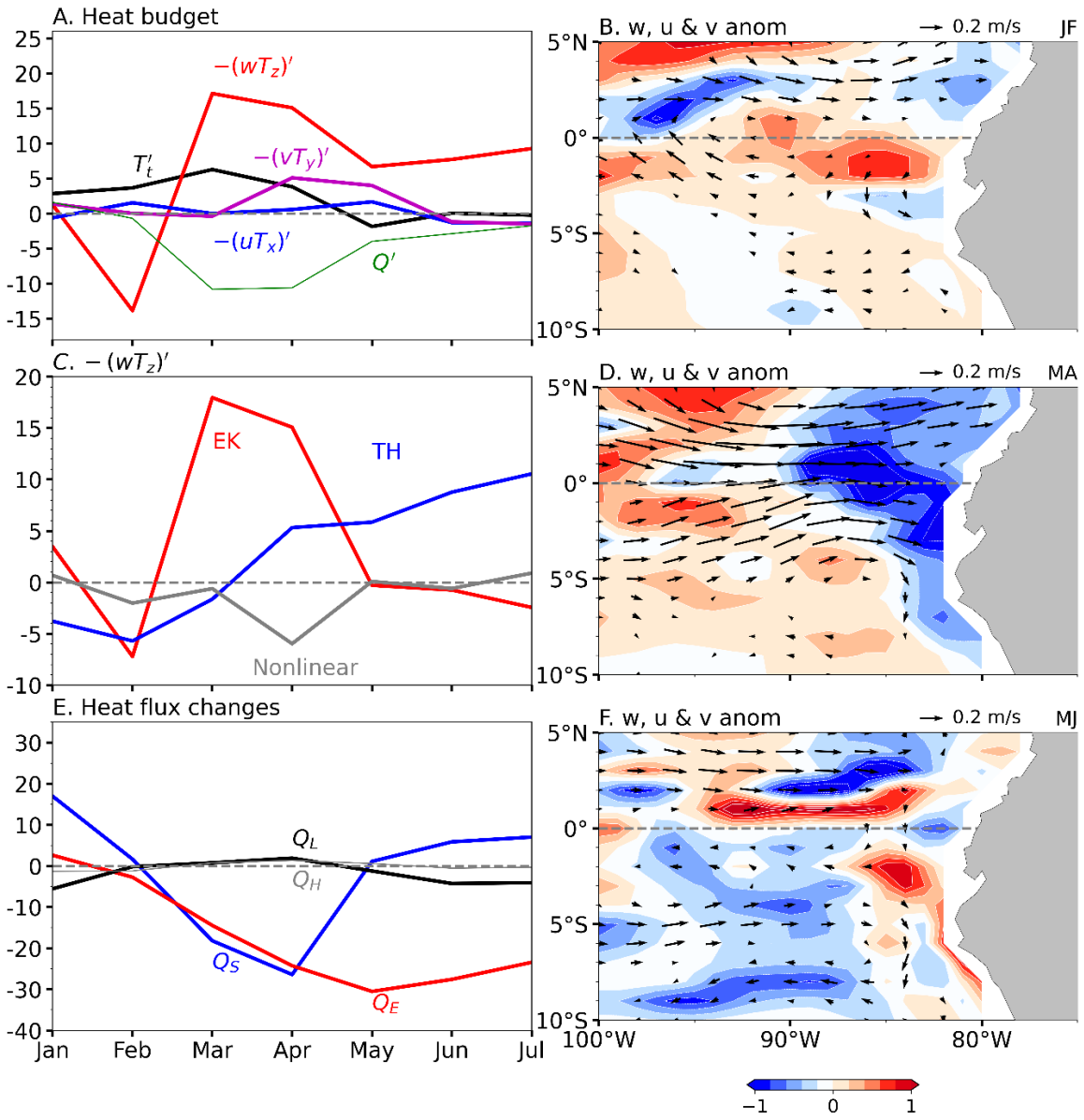

fig. S6. Role of thermodynamics in the 2023 coastal El Niño. (A) Heat budget terms of the 2023 coastal El Niño (10^{-7} °C/s, averaged in CSA region) (see Materials and Methods). (C) The decomposition of the vertical advection term into thermocline feedback (TH, blue line), Ekman feedback (EK, red line), and the nonlinear term (grey line). (E) Changes in each heat flux component in 2023, where Q_S represents surface solar radiation, Q_E denotes latent heat flux, Q_L represents longwave radiation, and Q_H represents sensible heat flux. (Right panels) Spatial pattern of the vertical velocity anomalies at the mixed layer bottom (color shading, 10^{-5} m/s) and mixed layer horizontal current anomalies (vectors, m/s) averaged during (B) January-February, (D) March- April, and (F) May-June of 2023.

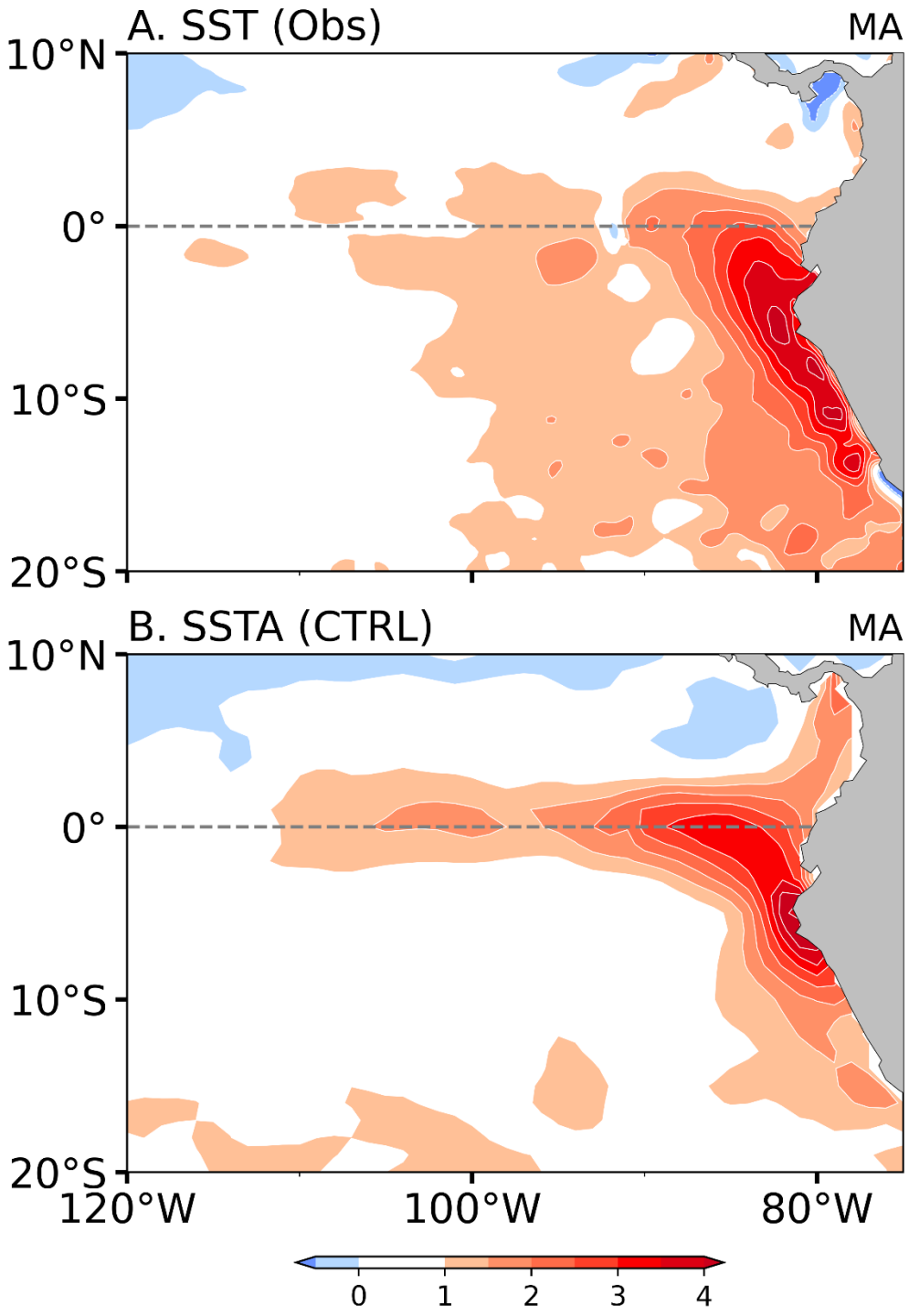

fig. S7. Comparison of observed and simulated SSTA for the 2023 coastal El Niño. March-April (MA) averaged (A) observed and (B) MITgcm simulated (CTRL run) SSTA (°C) in 2023.

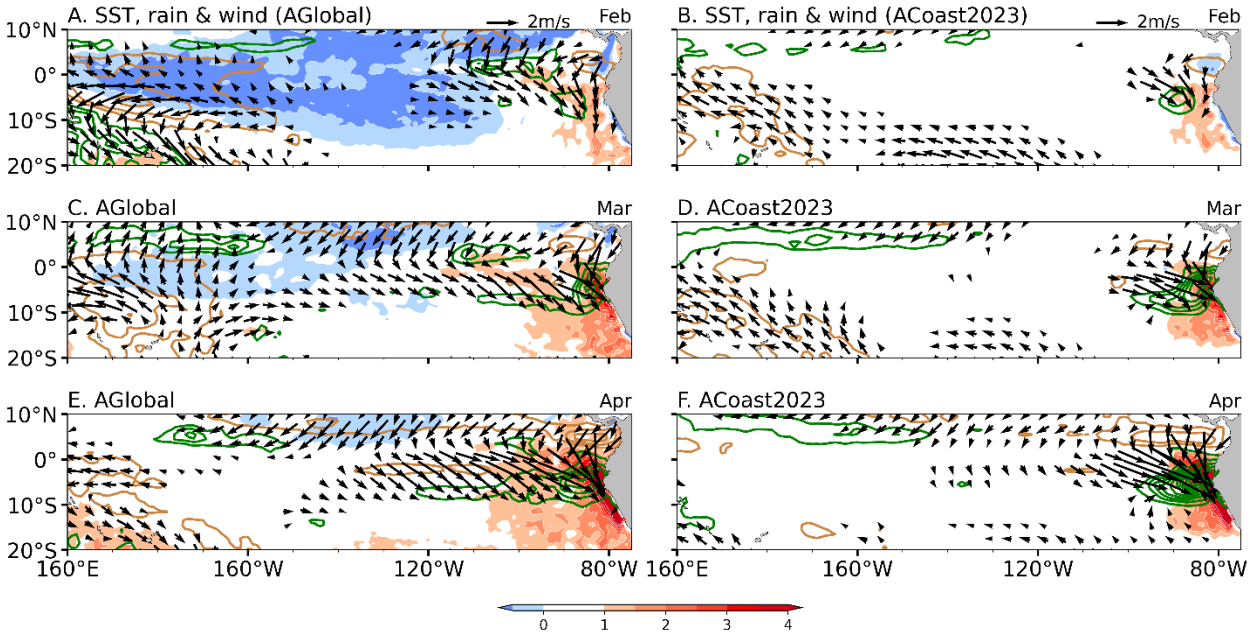

fig. S8. The simulated atmospheric responses to the 2023 coastal El Niño. (Left panels) SST anomalies (℃, color shading), 10-m wind (m/s, vectors; values below 0.5 m/s not shown), and rainfall anomalies (line contours with an interval of 2 mm/day; positive values in green and negative values in brown) during (A) February, (C) March, and (E) April in AGlobal. (Right panels) Same as (Left panels) but for the outputs from the ACoast2023 experiment.

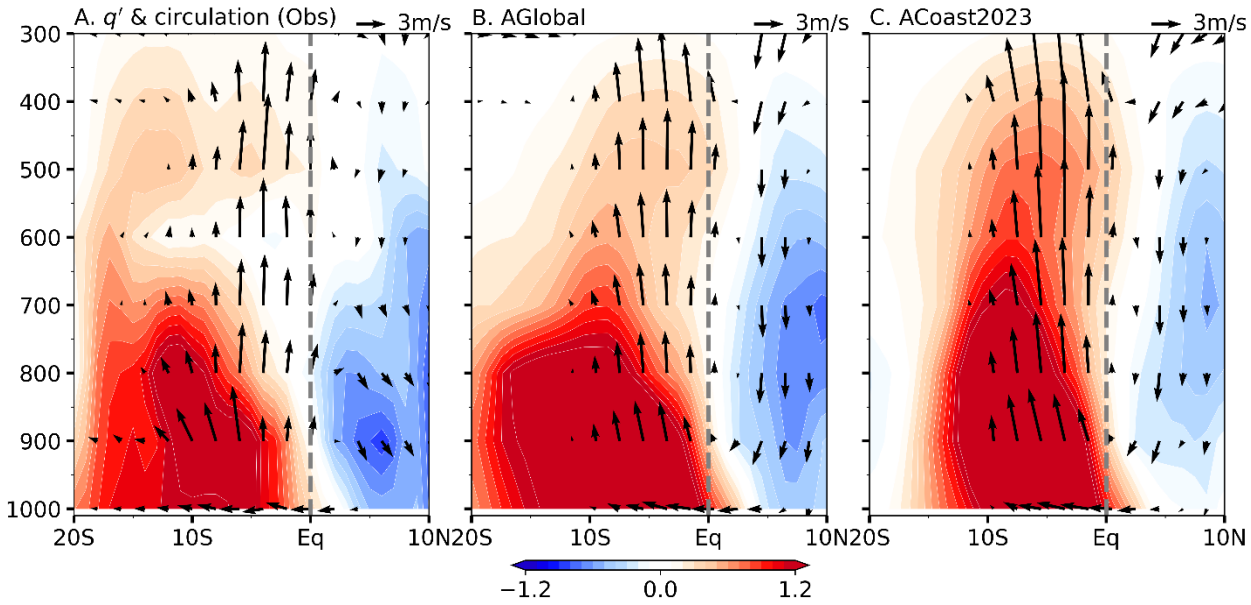

fig. S9. Atmospheric Response to Coastal SSTAs of 2023. (a) Anomalies in Vertical Circulation (vectors; m/s; magnified by a factor of 100 for visualization purposes) and Specific Humidity (q', g/kg; represented by color shading) across the Eastern Pacific (zonally averaged between 80°W and 85°W) as derived from (A) observations, (B) AGlobal, and (C) ACoast2023 experiments.

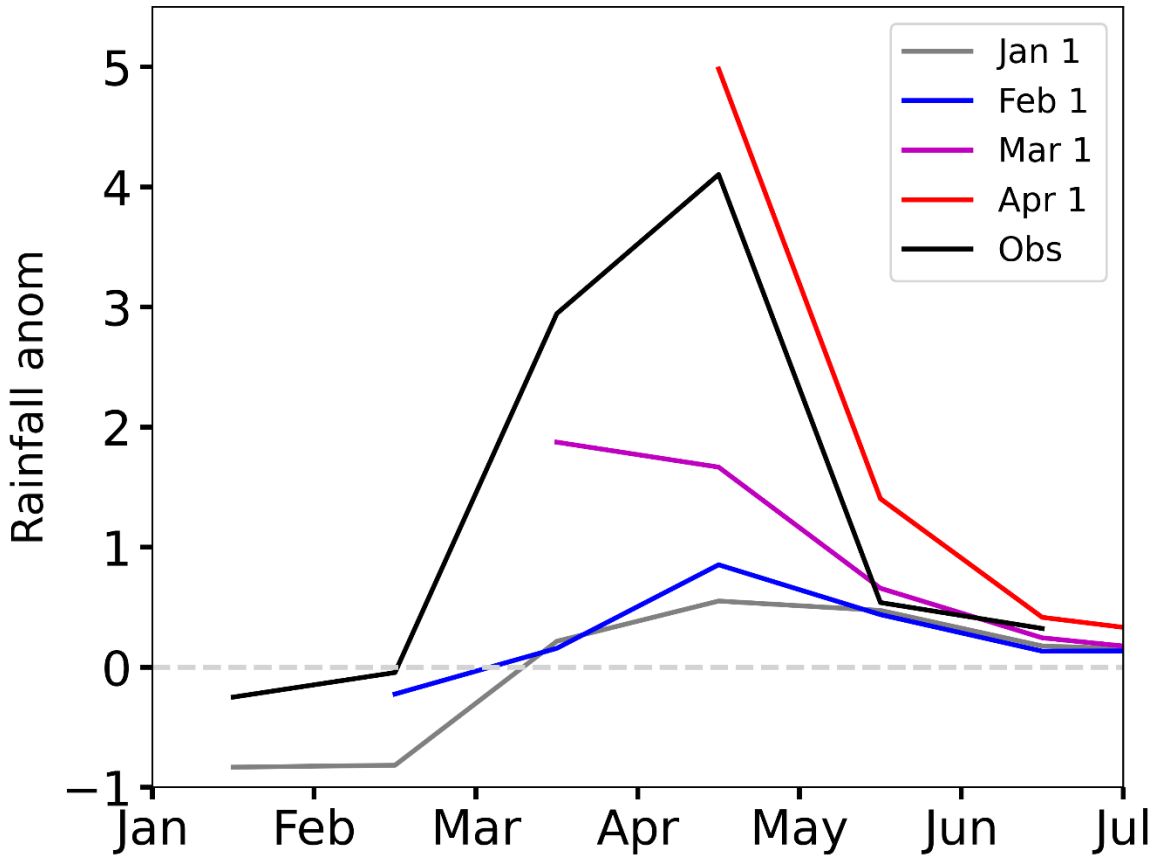

fig. S10. Predictions of the 2023 extreme coastal rainfall from the NMME. CSA anomalous rainfall (mm/day) forecasts initialized on 1 January 2023 (grey),1 February 2023 (blue), 1 March 2023 (magenta), and 1 April 2023 (red). Also plotted in black are observations.

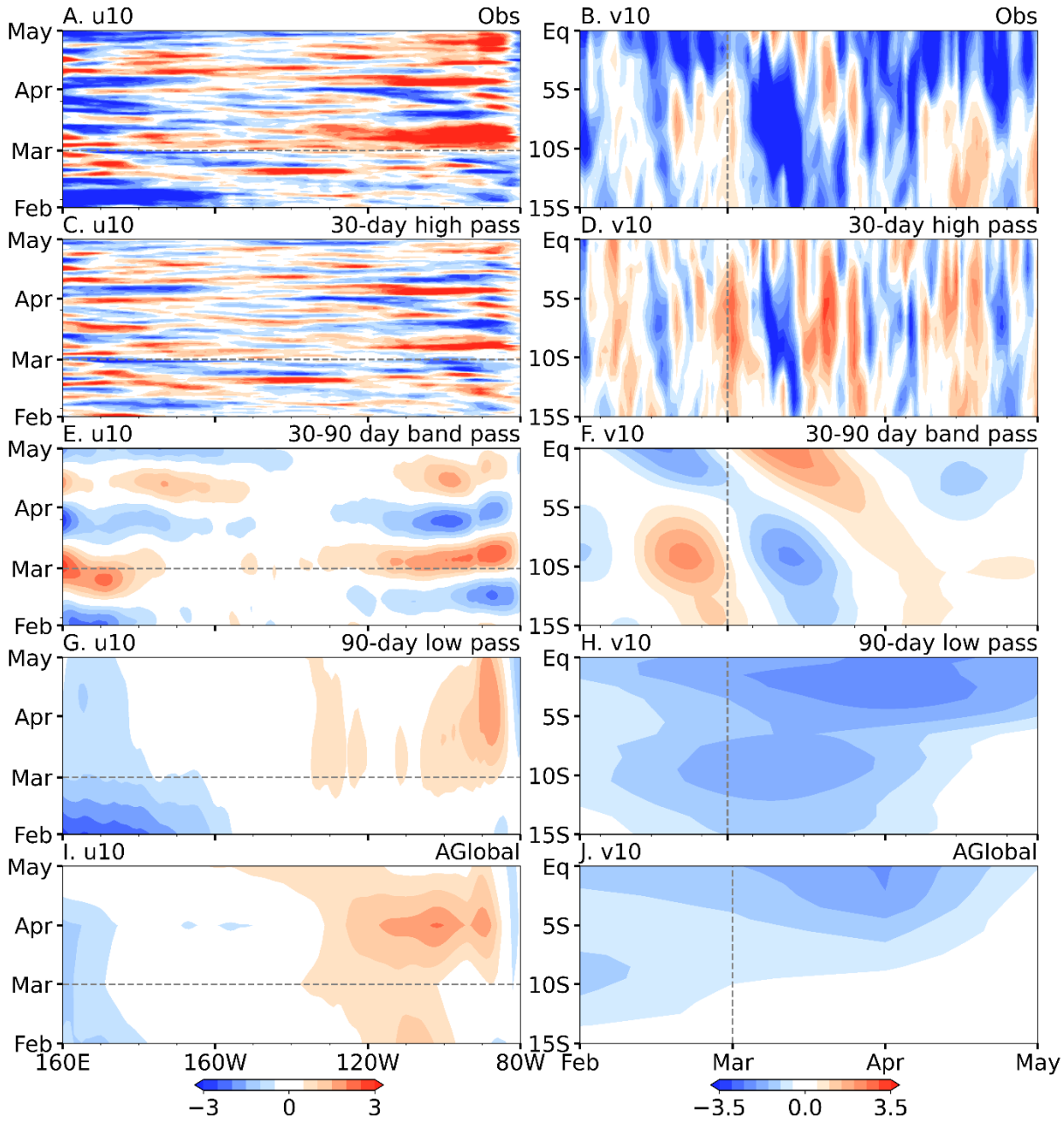

fig. S11. Hovmöller diagram of 10-m wind anomalies in 2023 at different timescales. (A) Longitude-time evolution of observed equatorial u10 anomalies (m/s). (C), (E), and (G) same as (A) but for the 30-day high pass, 30–90-day band pass, and 90-day low pass filtered u10 anomalies, respectively. (I) Same as (A) but from the AGlobal experiment. (Right panels) Same as (Left panels) but for latitude-time evolution of the coastal v10 anomalies (zonally averaged over 80°W-85°W).

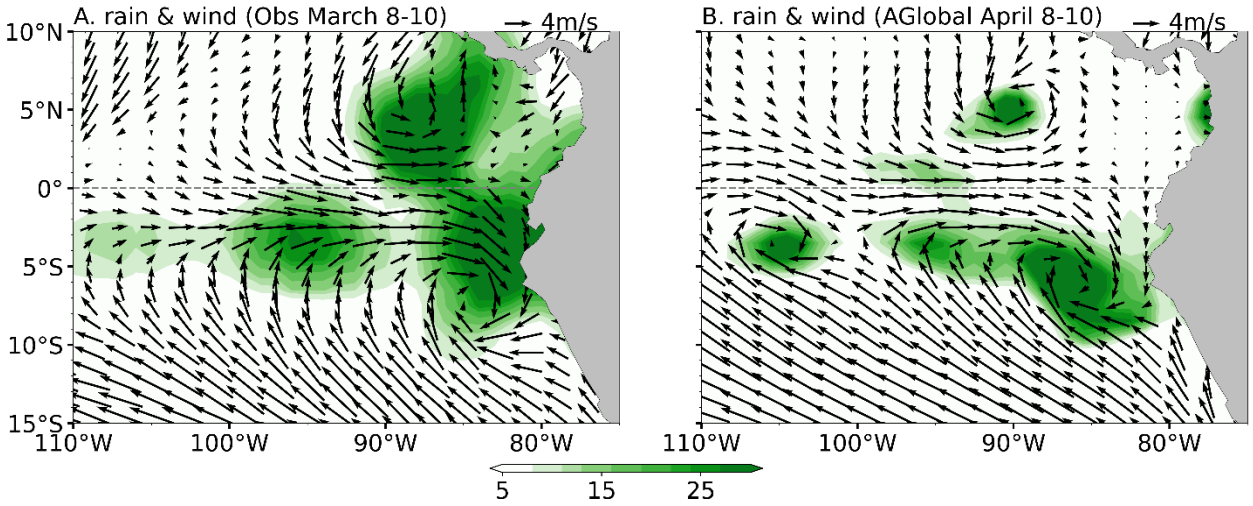

fig. S12. Observed and simulated tropical depressions in 2023. Rainfall (mm/day, color shading) and 10-m wind (m/s, vectors) averaged during (A) March 8-10, 2023 from observations and (B) April 8-10, 2023 in the 10th member run with large CSA v10 spread of AGlobal.

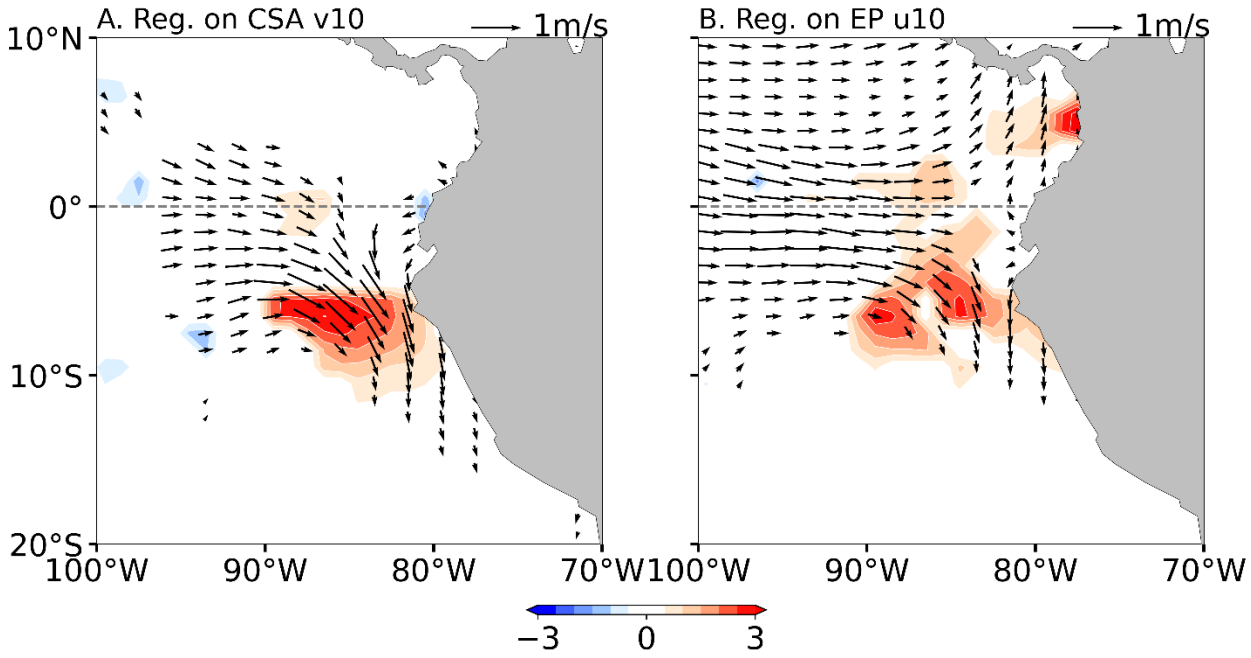

fig. S13. Atmospheric anomalies associated with internal variability in AGlobal. (A) Regression (sign reversed) of rainfall (shading, mm/day) and 10-m wind (vector, m/s) anomalies onto 2023 MA CSA v10 ensemble spread variability from AGlobal. (B) Same as (A), but for regression on the EP u10 ensemble spread variability. Here, the ensemble spread variability is obtained by subtracting the ensemble mean from each individual member.